

Revealing the pH Dependent Activities and Surface Instabilities for Ni-based Electrocatalysts during the Oxygen Evolution Reaction

Chunzhen Yang, Maria Batuk, Quentin Jacquet, Gwenaëlle Rouse, Wei Yin, Leiting Zhang, Joke Hadermann, Artem Abakumov, Giannantonio Cibin, Alan V. Chadwick, Jean-Marie Tarascon, and Alexis Grimaud

ACS Energy Lett., **Just Accepted Manuscript** • DOI: 10.1021/acsenergylett.8b01818 • Publication Date (Web): 05 Nov 2018

Downloaded from <http://pubs.acs.org> on November 5, 2018

Just Accepted

“Just Accepted” manuscripts have been peer-reviewed and accepted for publication. They are posted online prior to technical editing, formatting for publication and author proofing. The American Chemical Society provides “Just Accepted” as a service to the research community to expedite the dissemination of scientific material as soon as possible after acceptance. “Just Accepted” manuscripts appear in full in PDF format accompanied by an HTML abstract. “Just Accepted” manuscripts have been fully peer reviewed, but should not be considered the official version of record. They are citable by the Digital Object Identifier (DOI®). “Just Accepted” is an optional service offered to authors. Therefore, the “Just Accepted” Web site may not include all articles that will be published in the journal. After a manuscript is technically edited and formatted, it will be removed from the “Just Accepted” Web site and published as an ASAP article. Note that technical editing may introduce minor changes to the manuscript text and/or graphics which could affect content, and all legal disclaimers and ethical guidelines that apply to the journal pertain. ACS cannot be held responsible for errors or consequences arising from the use of information contained in these “Just Accepted” manuscripts.

1
2
3
4 **Revealing the pH Dependent Activities and Surface Instabilities for Ni-based**
5
6 **Electrocatalysts during the Oxygen Evolution Reaction**
7
8
9

10 Chunzhen Yang,^a Maria Batuk,^b Quentin Jacquet,^a Gwenaëlle Rouse,^{acd} Wei Yin,^a
11
12 Leiting Zhang,^a Joke Hadermann,^b Artem M. Abakumov,^c Giannantonio Cibin,^f Alan
13
14 Chadwick,^g Jean-Marie Tarascon,^{acdh} and Alexis Grimaud^{*acd}
15
16
17
18

19 ^a Chimie du Solide et de l'Energie, Collège de France, UMR 8260, 75231 Paris Cedex
20
21 05, France
22

23 ^b EMAT, University of Antwerp, Groenenborgerlaan 171, B-2020 Antwerp, Belgium
24
25

26 ^c Réseau sur le Stockage Electrochimique de l'Energie (RS2E), CNRS FR3459, 33
27
28 rue Saint Leu, 80039 Amiens Cedex, France
29

30 ^d Department of Chemistry, UPMC, 4 Place Jussieu, 75005 Paris, France
31
32

33 ^e Skoltech Center for Electrochemical Energy Storage, Skolkovo Institute of Science
34
35 and Technology, Moscow 143026, Russia
36

37 ^f Diamond Light Source, Harwell Science and Innovation Campus, Didcot,
38
39 Oxfordshire OX11 0DE, U.K.
40

41 ^g School of Physical Sciences, University of Kent, Canterbury, Kent CT2 7NH, U.K.
42
43

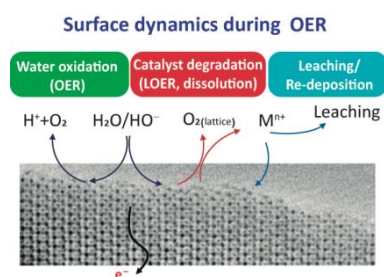
44 ^h ALISTORE-European Research Institute, FR CNRS 3104, 80039 Amiens, France
45
46
47

48
49 email: alexis.grimaud@college-de-france.fr
50
51
52
53
54
55
56
57
58
59
60

Abstract

Multiple electrochemical processes are involved at the catalyst/electrolyte interface during the oxygen evolution reaction (OER). With the purpose of elucidating the complexity of surface dynamics upon OER, we systematically studied two Ni-based crystalline oxides ($\text{LaNiO}_{3-\delta}$ and $\text{La}_2\text{Li}_{0.5}\text{Ni}_{0.5}\text{O}_4$) and compared them with the state-of-the-art Ni-Fe (oxy)hydroxide amorphous catalyst. Electrochemical measurements such as rotating ring disk electrode (RRDE) and electrochemical quartz microbalance microscopy (EQCM), coupled with a series of physical characterizations including transmission electron microscopy (TEM) and X-ray absorption spectroscopy (XAS) are conducted to unravel the exact pH effect on both the OER activity and the catalyst stability. We demonstrate that for Ni-based crystalline catalysts the rate for surface degradation depends on the pH and is greater than the rate for surface reconstruction. This behavior is unlike for amorphous Ni oxyhydroxide catalyst which is found more stable and pH independent.

TOC



1
2
3
4 Water splitting is considered as a promising strategy to store energy from renewable
5
6 energies in the form of a fuel (H_2) and has therefore attracted tremendous attention in
7
8 recent years.¹⁻² Nevertheless, the sluggish kinetics of the half reaction occurring at
9
10 the anode, namely the oxygen evolution reaction (OER), currently limits the
11
12 efficiency of the overall process, hence calling for the development of better
13
14 electrocatalysts. Despite recent successes at designing earth-abundant crystalline or
15
16 amorphous transitional metal oxides and oxyhydroxides,³⁻⁶ our understanding of the
17
18 active catalysts' structure and structural stability is still insufficient.

21
22 The activity of lattice oxygen for participating the in the OER has previously been
23
24 investigated by isotopic labeling experiments coupled with differential electrochemical mass
25
26 spectroscopy (DEMS) on RuO_2 ⁷ and on Au electrode⁸. Results showed that O-O bonds could
27
28 be formed between the lattice oxygen and surface absorbed oxygen, following a mechanism
29
30 which can be compared to the well-known Mars-Van Krevelen (MvK) mechanism previously
31
32 described for gas phase catalysis.⁹ Recent discoveries further pointed towards common
33
34 intermediates responsible for the involvement of lattice oxygen into the OER mechanism⁷⁻⁸
35
36 but also into the surface degradation.^{6, 10-13} Moreover, triggering the redox activity of
37
38 lattice oxygen was found to often be associated with a strong pH dependence for the
39
40 anodic current,¹⁴⁻¹⁷ suggesting either a decoupled proton-electron-transfer mechanism
41
42 for which the rate-determining step is shifting from the formation of O-O bonds to the
43
44 deprotonation of $OH_{(ads)}$ or $OOH_{(ads)}$, or the chemical formation of pre-catalyst as
45
46 being rate limiting. In any case, it was further demonstrated that the proton transfer
47
48 kinetics at the catalyst/electrolyte interface becomes limiting for a wide variety of
49
50 OER catalysts.¹⁸⁻¹⁹ However, when the kinetics for refilling oxygen vacancies is slow,
51
52 instability for oxide catalysts is often observed.^{3, 20-21} This instability originates from
53
54 cation dissolution which is triggered by the lowering of their coordination, hence
55
56 often resulting in a rapid surface amorphization accompanied with a change of the
57
58
59
60

1
2
3
4 oxidation state for the transition metal on the surface, which led researchers to term
5 these catalysts as redox active.²²⁻²³ From these recent findings, understanding the
6 delicate equilibriums existing on the surface of crystalline transition metal oxides
7
8 appears to be vital for the development of efficient and stable OER catalysts. This is
9
10 particularly true following recent knowledge developed for electrodeposited catalysts
11
12 such as Co phosphate (CoP_i)²⁴⁻²⁵ or Ni-Fe oxyhydroxide (Ni_{1-x}Fe_xOOH)^{17, 26} for which
13
14 a constant dissolution/redeposition process involved in the OER, also often poised as
15
16 self-healing mechanism, places them at the border between solid heterogeneous and
17
18 molecular homogenous catalysts.
19
20
21
22

23
24 In detail, the rapid surface reconstruction occurring for some oxide catalysts during
25
26 the OER may involve multiple steps, including water adsorption and oxidation
27
28 followed by oxygen release²⁷, catalyst degradation and cation dissolution induced by
29
30 the evolution of lattice oxygen, the subsequent re-deposition process and the
31
32 formation of amorphous surface with a structure often resembling that of
33
34 (oxy)hydroxide-like species. So far, the complexity of the surface dynamics and our
35
36 poor knowledge of the kinetics associated with each step hampered our understanding
37
38 of the OER mechanism²⁸, hence calling for a protocol to accurately study these
39
40 catalysts. This is especially true regarding the exact effect of pH which, by modifying
41
42 the different equilibriums occurring at the catalyst/electrolyte interface, can impact
43
44 both the activity and the stability of the catalysts.¹⁷
45
46
47

48
49 With the purpose of unveiling the pH effect on the underlying OER mechanism, we
50
51 developed a redox active OER catalyst La₂Li_{0.5}Ni_{0.5}O_{4±δ} (LLNO) with
52
53 Ruddlesden-Popper (RP) structure in which Li⁺ serves as sacrificial cation that
54
55 leaches out under OER conditions to activate the redox activity of the surface and
56
57 initiate further surface degradation that we aim at studying in this work. This RP-type
58
59 LLNO phase was designed as a redox active Ni³⁺ counterpart to LaNiO_{3-δ} which was
60

1
2
3
4 previously suggested to undergo lattice oxygen oxidation and evolution.²¹ We then
5
6 systematically studied the physical and electrochemical properties of these two
7
8 Ni-based crystalline oxides and compared them with the state-of-the-art Ni-Fe
9
10 (oxy)hydroxide ($\text{Ni}_{1-x}\text{Fe}_x\text{OOH}$) amorphous catalyst^{26, 29} (Supplementary Figure S1).
11
12 Coupling electrochemical tools such as rotating ring disk electrode (RRDE)³⁰⁻³¹ and
13
14 electrochemical quartz microbalance microscopy (EQCM) with physical
15
16 characterizations such as X-ray diffraction (XRD), transmission electron microscopy
17
18 (TEM), and X-ray absorption spectroscopy (XAS) at Ni K-edge, we discuss in this
19
20 study the exact effect of pH on both the OER activity and the catalyst stability for
21
22 each of these different classes of compounds.
23
24
25
26
27

28
29 The structures of LLNO and $\text{LaNiO}_{3-\delta}$ were first examined using Rietveld refinements
30
31 of data from laboratory XRD measurements (Figure 1a and Figure S1). The LLNO
32
33 compound shows the Ruddlesden-Popper structure with a space group of $I4/mmm$,
34
35 indicative of a disordering of NiO_6 and LiO_6 octahedra sharing corners and forming
36
37 layers along the ab plane in between which La^{3+} cations occupy a position with 9-fold
38
39 coordination.³² $\text{LaNiO}_{3-\delta}$ possesses the rhombohedral perovskite structure with 3D
40
41 arrangement of corner-shared NiO_6 octahedra. In contrary, the amorphous and
42
43 electrodeposited Ni (oxy)hydroxide is composed of units of less than 10 edge-shared
44
45 NiO_6 octahedra with terminal under-coordinated oxygen, as previously refined by
46
47 XAS measurements.^{29, 33-34}
48
49
50
51
52
53
54
55
56
57
58
59
60

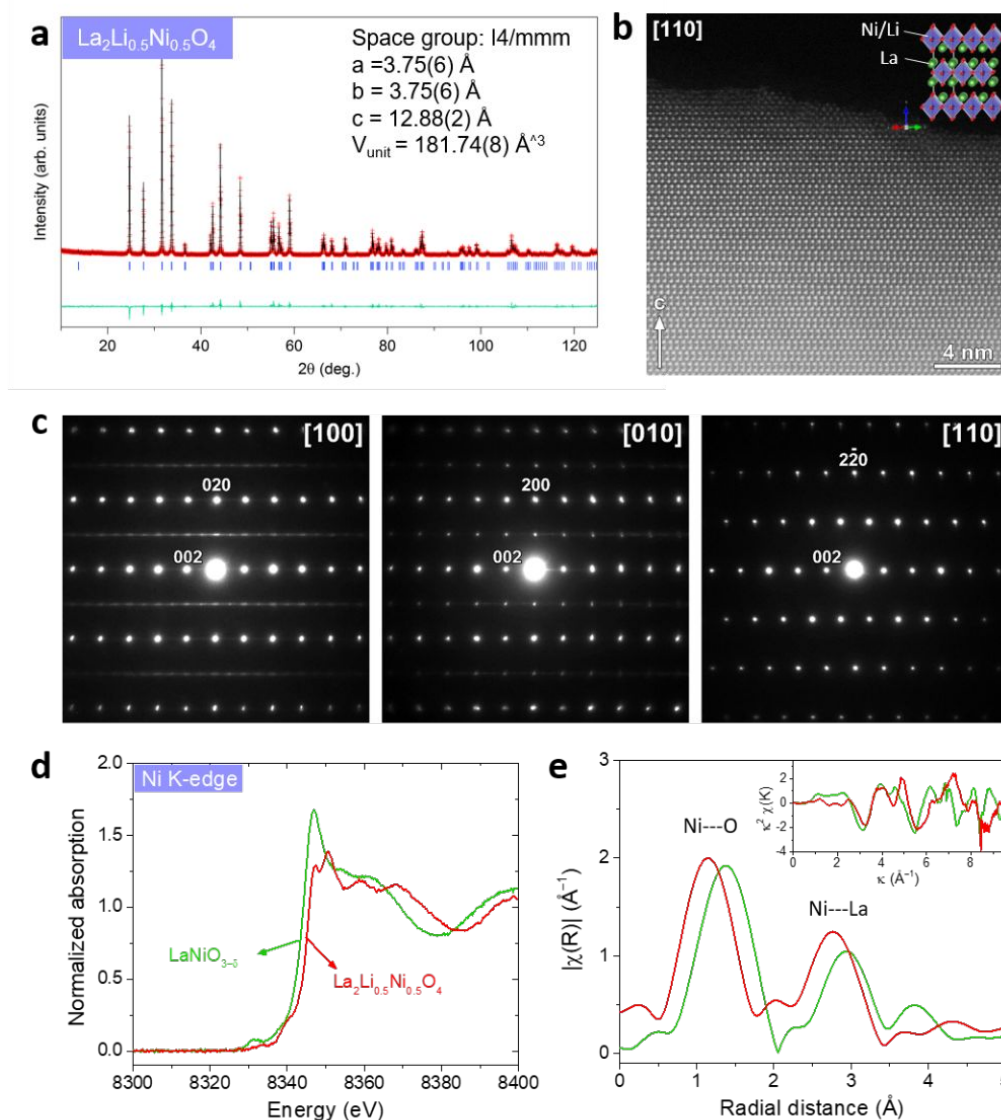


Figure 1. Structural characterizations of $\text{La}_2\text{Li}_{0.5}\text{Ni}_{0.5}\text{O}_4$. (a) X-ray powder diffraction pattern with Rietveld refinement. (b) [110] high-resolution HAADF-STEM image showing the structure of $\text{La}_2\text{Li}_{0.5}\text{Ni}_{0.5}\text{O}_4$. (c) Electron diffraction patterns along [100], [010], and [110] directions for $\text{La}_2\text{Li}_{0.5}\text{Ni}_{0.5}\text{O}_4$. (d) Ni K-edge XANES absorption spectra recorded for $\text{La}_2\text{Li}_{0.5}\text{Ni}_{0.5}\text{O}_4$ and $\text{LaNiO}_{3-\delta}$. (e) Magnitude of Fourier transform of k^3 -weighted EXAFS oscillations for the pristine $\text{La}_2\text{Li}_{0.5}\text{Ni}_{0.5}\text{O}_4$ and $\text{LaNiO}_{3-\delta}$. In inset is shown the EXAFS oscillations in k -space.

Following this structural determination, the Ni oxidation state for crystalline LLNO and $\text{LaNiO}_{3-\delta}$ was determined by the means of Ni K-edge XAS spectroscopy (Figure

1
2
3
4 1d-e). When compared to $\text{LaNiO}_{3-\delta}$, a slight shift towards higher energy for the Ni
5
6 K-edge was measured for LLNO, suggesting a slightly higher Ni oxidation state
7
8 which could be explained by the presence of oxygen vacancies in $\text{LaNiO}_{3-\delta}$, as often
9
10 reported for as synthesized compound.³⁵ The crystal structure of LLNO was further
11
12 confirmed by TEM: high-angle annular dark-field scanning transmission electron
13
14 microscopy (HAADF-STEM) images visualize the cations arrangement in the LLNO
15
16 structure (Figures 1b, S2 and S3) and show a clean surface with only a very thin
17
18 amorphous layer of 0.5 nm. Furthermore, while laboratory XRD was showing an
19
20 average disordering of Li and Ni, electron diffraction patterns (Figure 1c) shows
21
22 crystallites with a local ordering of NiO_6 and LiO_6 octahedra, confirming the *Ammm*
23
24 symmetry and lattice parameters previously proposed. Finally, the $0kl: k+l=2n+1$
25
26 reflections in the $[100]$ patterns are due to twinning with $[010]$.
27
28
29

30 Figure S4-S5 shows the electrochemical activity under OER conditions normalized by
31
32 surface area as deduced by Brunauer, Emmet, Teller (BET) measurements for LLNO
33
34 and $\text{LaNiO}_{3-\delta}$ and compared to the one measured for the nickel (oxy)hydroxide film as
35
36 normalized by geometric surface area. Similar anodic currents as well as Tafel slopes
37
38 were obtained for LLNO and $\text{LaNiO}_{3-\delta}$ after the first cycle, suggesting similar OER
39
40 mechanism and kinetics for these two crystalline Ni-based compounds.
41
42
43

44 RRDE measurements³⁰⁻³¹ were further carried out to better understand the effect of
45
46 pH on the anodic current, and more specifically the current resulting from the oxygen
47
48 evolution on the surface of the catalyst from the contribution arising from catalyst
49
50 degradation (Figure 2 and Figure S6). By calculating the collection efficiency
51
52 $\eta = (i_{ring}/i_{disc})$ at a fixed potential ($E = 1.6$ V vs. RHE) at which the oxygen
53
54 evolution occurs, the effective current contributing from oxygen evolution can thus be
55
56 estimated.³⁰ The RRDE study reveals that the OER activity for both LLNO and
57
58 $\text{LaNiO}_{3-\delta}$ increases with the pH while it remains mostly constant for the amorphous
59
60

film (Figure 2c). The collection efficiency for both LLNO and $\text{LaNiO}_{3-\delta}$ was found to decrease with pH from around 10% at pH 12.5 to around 5% at pH 14 (Figure 2e). In contrast, while the collection efficiency was also found to be close to 10% at pH 12.5 for the Ni(Fe)OOH film after 10 cycles, very stable OER performances and contribution from the oxygen evolution to the anodic current were found for this catalyst at every pH (Figure 2e).

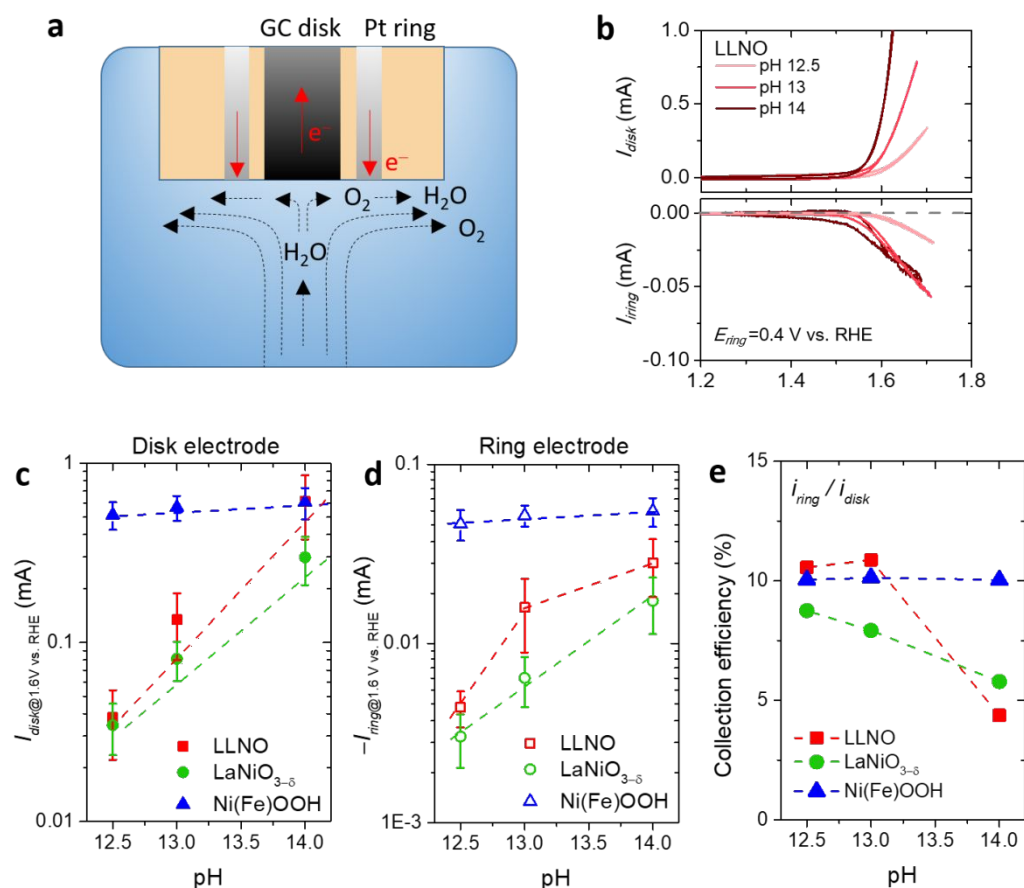


Figure 2. pH dependent activity and O₂ evolution efficiency studied by the RRDE measurement. (a) scheme for the RRDE experiment. (b) Results obtained for LLNO at pH 12.5, 13 and 14. (c) pH dependent OER activities with stabilized current measured by the disk electrode after activation for 10 cycles at a working potential of 1.6 V vs. RHE. (d) the corresponding ring current, and (e) the collection efficiency ($\eta = i_{ring}/i_{disk}$). The collection efficiency (η) of the RRDE system is estimated to be around 10% as obtained on the electrodeposited Ni(Fe)OOH film catalyst (see methods in the Supplementary Information).

1
2
3
4
5
6 Observing that the anodic current for LLNO was found to increase with cycling at pH
7
8 13 while it was found stable for the two other Ni-based catalysts at every pH (Figure
9
10 S7), we further investigated the effect of cycling on the collection efficiency as a
11
12 function of pH (Figure 3). The three Ni-based model catalysts were found to
13
14 demonstrate contrasted stability features when cycling at different pH. For the LLNO
15
16 sample, an activation process at pH 12.5 and pH 13 during the initial 10 cycles is
17
18 observed, with the collection efficiency (η) increasing from ~6% up to 12%. The low
19
20 collection efficiency in the initial 1-3 cycles may be ascribed to the redox process
21
22 induced by the gradual leaching of cations from the LLNO structure, whereas the high
23
24 value of η obtained after activation would be a strong indication for a stable oxygen
25
26 evolution current. However, when cycling LLNO at pH 14, poor oxygen evolution
27
28 with a collection efficiency lower than 5% was found, suggesting that the main
29
30 contribution to the anodic current originates from parasitic oxidation/corrosion
31
32 phenomenon. We could further detect a continuous loss of electrochemically active
33
34 surface area for LLNO at pH 14 as seen by the gradual decrease of the
35
36 pseudocapacitive contribution upon cycling (Figure S9-10). For the $\text{LaNiO}_{3-\delta}$ sample,
37
38 after an initial drop for the first few cycles, the ring current for oxygen detection and
39
40 the collection efficiency are found relatively stable at each pH during cycling,
41
42 suggesting that the rate for parasitic oxidative reaction during OER is very slow.
43
44 Nevertheless, the overall collection efficiency was found to decrease with pH which
45
46 suggests that the pH affects the degradation rate which gets stronger at higher pH. On
47
48 the other hand, for Ni(Fe)OOH the disk current, ring current and the collection
49
50 efficiency are found fairly stable upon cycling and they show no dependence on the
51
52 pH.
53
54
55
56
57
58
59
60

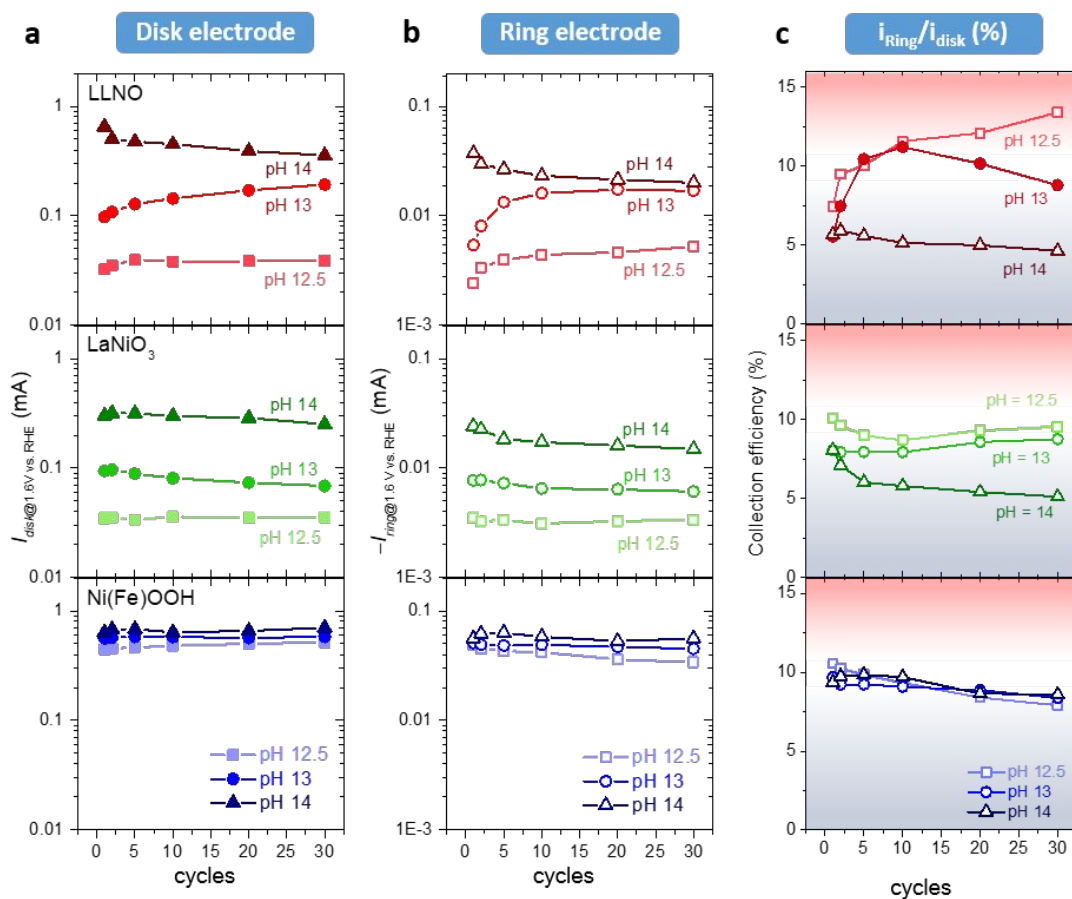


Figure 3. Electrochemical stability for the three nickel base catalysts versus cycling and pH: LLNO, LaNiO_{3-δ}, and Ni(Fe)OOH. The disk current (a), ring current (b), and the collection efficiency (c) are plotted vs. the cycling number. The low collection efficiency ($\eta < 8\%$) is ascribed to the significant degradation process such as cation dissolution.

Therefore, the anodic current measured for the amorphous film arises from oxygen evolution, whereas for crystalline nickel-based oxides a non-negligible part of the current originates from a catalyst degradation process which is enhanced at high pH. We could finally show that the decreased collection efficiency found for LLNO and LaNiO_{3-δ} with pH is not arising from the use of carbon additive by showing that the collection efficiency measured for Ni(Fe)OOH is not affected by the addition of carbon (Figure S8).³⁶ This is consistent with the observation that the pseudocapacitive

1
2
3
4 current decreases for LLNO with cycling (Figure S9-10) while the collection
5 efficiency is found rather constant (Figure 3c), indicative of a reduction of the
6 electrochemically active surface area due to surface degradation while the part of the
7 anodic current arising from the OER remains almost constant.
8
9

10
11
12 We further probe the degradation process occurring for these catalysts by the means
13 of electrochemical quartz crystal microbalance (EQCM) (Figure 4). Using this
14 weight-sensitive technique, we could conclude that the $\text{LaNiO}_{3-\delta}$ catalyst shows only a
15 very limited mass loss during OER cycling at pH 13, with a slight drop of its mass
16 observed at high potential. Similar observation was made for the amorphous
17 Ni(Fe)OOH film. On the contrary, a severe mass loss is recorded for LLNO, this loss
18 being potential-dependent and occurring above 1.5 V vs. RHE in the water oxidation
19 region. Overall, a mass loss higher than 10 wt.% could be observed after 30 cycles,
20 the first cycle accounting for most of this loss which gradually slows down during the
21 subsequent cycles. Repeating these EQCM measurements at varied pH for LLNO
22 (Figure S12), it is observed that the mass loss increases with pH. This observation is
23 consistent with the RRDE results discussed above, and indicates that surface
24 degradation is pH dependent for this nickel-based Ruddelsden-Popper oxide. A
25 reversible evolution of lattice oxygen, the mechanism often proposed for the redox
26 active compounds, would be counter-balanced by water adsorption and should not
27 lead to any mass loss. Our results clearly show that this redox process is accompanied
28 with drastic degradation for the LLNO catalyst.
29
30
31
32
33
34
35
36
37
38
39
40
41
42
43
44
45
46
47
48
49
50
51
52
53
54
55
56
57
58
59
60

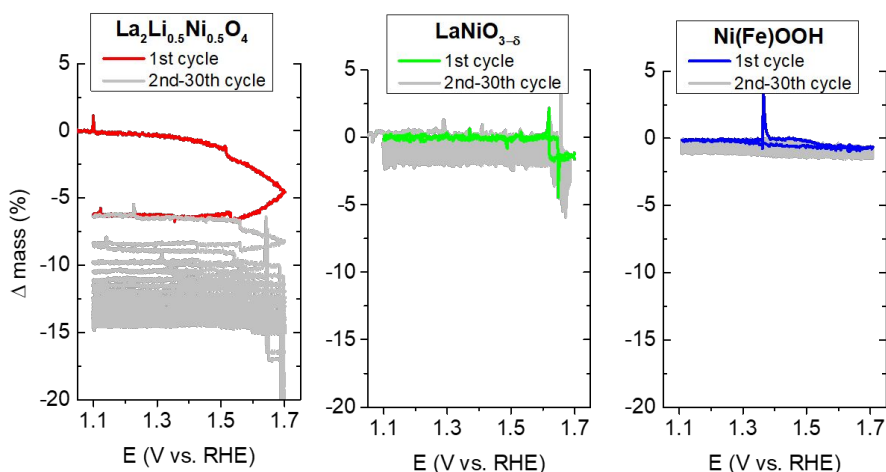


Figure 4. Comparison of the mass loss of $\text{LaNiO}_{3-\delta}$, $\text{La}_2\text{Li}_{0.5}\text{Ni}_{0.5}\text{O}_4$ and $\text{Ni}(\text{Fe})\text{OOH}$ hydroxide catalysts upon cycling in KOH solution ($\text{pH} = 13$) recorded by electrochemical quartz crystal microbalance (EQCM).

We further studied the surface properties of the cycled LLNO and $\text{LaNiO}_{3-\delta}$ samples by HAADF-STEM and XAS at the Ni K-edge (Figure 5). A thin amorphous layer was observed on cycled LLNO samples (after 30 CV cycles), as revealed by HAADF-STEM (Figure 5a), the thickness of which grows from ≈ 2 to 6 nm when increasing the pH from 12.5 to 14. To grasp more information about the surface amorphization process, XAS at Ni K-edge was conducted in both bulk-sensitive fluorescence yield (FY) mode and surface-sensitive total electron yield (TEY) mode (Figure 5b and 5d, respectively). No significant modification of the Ni oxidation state after cycling is observed at each pH when compared to the pristine sample, unlike what could be observed for other redox active perovskites such as $\text{Ba}_{0.5}\text{Sr}_{0.5}\text{Co}_{0.8}\text{Fe}_{0.2}\text{O}_{3-\delta}$.^{6, 37} The corresponding EXAFS spectra also confirmed that the atomic local environment on the surface of this oxide is maintained upon cycling, with the apparition of a new feature at around 2 Å in reduced distances which would correspond to an edge-shared octahedra coordination growing with pH. EDX analysis was then conducted to provide information about the chemical compositions of the

amorphous film (Figure S13). When compared to the bulk crystals, the amorphous layer shows similar elemental distributions including Ni, La, and O. Recrystallization process of the surface is observed under the electron beam (Figure S13), with only a loss of long range order possibly due to atomic defects (vacancies) formed upon cycling. This observation indicates that not only Li is leached out during cycling, but that La and Ni cations are also continuously lost on the surface leading to a drastic loss of mass as shown by EQCM. Hence, these results show that the amorphous thin layer formed on the LLNO surface mostly originates from the redox activity of the surface, suggesting that the edge-shared octahedra motifs observed by EXAFS grow farther from the surface of the particles. Nevertheless, this result cannot explain the loss of more than 10% in mass of catalyst as recorded by EQCM (Figure 4a). Bearing in mind that the solubility of nickel in alkaline conditions is rather small, we hypothesize that clusters of nickel hydroxides could be formed in solution away from the electrode and do not deposit onto the surface of crystalline LLNO.

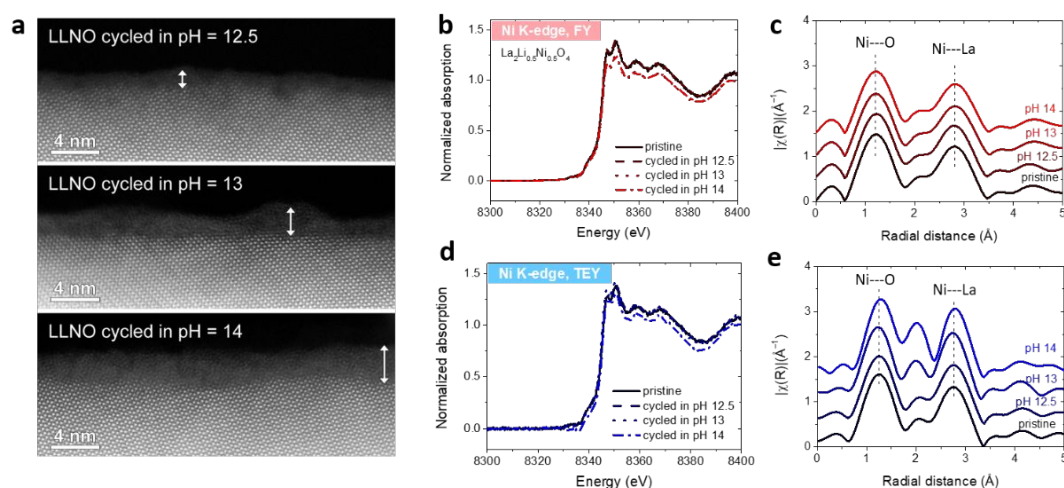


Figure 5. Surface deconstruction of $\text{La}_2\text{Li}_{0.5}\text{Ni}_{0.5}\text{O}_4$ catalyst. (a) HAADF-STEM images of cycled LLNO catalysts in KOH solutions at different pH. (b-e) Ni K-edge X-ray absorption spectra and the corresponding EXAFS oscillations recorded for LLNO after cycling in KOH solutions at different pH. (b) and (c) are recorded in the bulk-sensitive fluorescence mode (FY), (d) and (e) are recorded in surface-sensitive total electron

1
2
3 yield (TEY) mode.
4
5
6
7

8 As suggested in this work, the electrochemical activity and stability of oxide catalysts
9 are related to their crystal and electronic structures but also to the pH of the
10 supporting electrolyte. Using LLNO as a model compound, we show that pH
11 dependence for the anodic current measured with crystalline compounds can be
12 associated with severe surface degradation and lower oxygen evolution efficiencies,
13 unlike for amorphous catalysts. Combining post mortem analysis, we could explain
14 this phenomenon in terms of surface instability and degradation related to cations
15 leaching at high potential. Therefore, we believe that in order to accurately evaluate
16 the intrinsic OER activities of highly active oxide catalysts which may involve the
17 redox activity of lattice oxygen, it is essential to decouple the contributions of the
18 water oxidation and the oxygen evolution from the degradation processes associated
19 with catalyst degradation under anodic current. Toward this perspective, the use of
20 RRDE experiments appears as a promising strategy for accurately assessing the true
21 oxygen evolution contribution to the anodic current.³¹ In addition to RRDE, more
22 efforts should be devoted to developing proper characterizations for online detection
23 of gas evolution³⁸, mass dissolution³⁹, and intermediates formation by surface-enhanced
24 Raman spectroscopy⁴⁰ to provide more in-depth information about the complex surface
25 dynamics involved during the OER. We believe that this work will set up future
26 strategies to assess the real performances of potential OER catalysts and we can
27 foresee that catalyst structuration, which has been critical for developing advanced
28 oxygen reduction reaction (ORR) catalysts,⁴¹ will become even more important for
29 designing stable and active OER catalysts.
30
31
32
33
34
35
36
37
38
39
40
41
42
43
44
45
46
47
48
49
50
51
52
53
54
55
56
57
58
59
60

Acknowledgements

1
2
3
4 C.Y., J.-M.T. and A.G. acknowledge funding from the European Research Council
5 (ERC) (FP/2014)/ERC Grant-Project 670116-ARPEMA. A.G. acknowledges
6 financial support from the ANR MIDWAY (Project ID: [ANR-17-CE05-0008](#)). We
7
8 acknowledge Diamond Light Source for time awarded to the Energy Materials BAG
9
10 on Beamline B18, under Proposal sp12559.
11
12
13
14
15
16

17 **Supporting Information**

18
19 The Supporting Information is available free of charge on the ACS
20

21 Publications website at DOI: XXXX
22

23
24 Experiment description, more physical characterizations and electrochemical data
25
26 analyses are presented in the supporting information.
27
28
29
30

31 **References**

- 32
33 (1) Hunter, B. M.; Gray, H. B.; Muller, A. M., Earth-Abundant Heterogeneous Water
34 Oxidation Catalysts. *Chem. Rev.* **2016**, 116 (22), 14120-14136.
35
36 (2) Dau, H.; Limberg, C.; Reier, T.; Risch, M.; Roggan, S.; Strasser, P., The
37 Mechanism of Water Oxidation: From Electrolysis via Homogeneous to
38 Biological Catalysis. *ChemCatChem* **2010**, 2 (7), 724-761.
39
40 (3) Grimaud, A.; May, K. J.; Carlton, C. E.; Lee, Y. L.; Risch, M.; Hong, W. T.; Zhou, J.;
41 Shao-Horn, Y., Double Perovskites as a Family of Highly Active Catalysts for
42 Oxygen Evolution in Alkaline Solution. *Nat. Commun.* **2013**, 4, 2439.
43
44 (4) Mefford, J. T.; Rong, X.; Abakumov, A. M.; Hardin, W. G.; Dai, S.; Kolpak, A. M.;
45 Johnston, K. P.; Stevenson, K. J., Water Electrolysis on $\text{La}_{1-x}\text{Sr}_x\text{CO}_{3-\delta}$ Perovskite
46 Electrocatalysts. *Nat. Commun.* **2016**, 7, 11053.
47
48 (5) Yagi, S.; Yamada, I.; Tsukasaki, H.; Seno, A.; Murakami, M.; Fujii, H.; Chen, H.;
49 Umezawa, N.; Abe, H.; Nishiyama, N.; Mori, S., Covalency-reinforced Oxygen
50 Evolution Reaction Catalyst. *Nat. Commun.* **2015**, 6, 8249.
51
52 (6) Fabbri, E.; Nachttegaal, M.; Binniger, T.; Cheng, X.; Kim, B.-J.; Durst, J.; Bozza, F.;
53 Graule, T.; Schäublin, R. *et al.*, Dynamic Surface Self-reconstruction is the Key of
54 Highly Active Perovskite Nano-electrocatalysts for Water Splitting. *Nat. Mater.*
55 **2017**, 16 (9), 925-931.
56
57 (7) Macounova, K.; Makarova, M.; Krtil, P., Oxygen Evolution on Nanocrystalline
58
59
60

- 1
2
3 RuO₂ and Ru_{0.9}Ni_{0.1}O_{2-δ} Electrodes – DEMS Approach to Reaction Mechanism
4 Determination. *Electrochem. Commun.* **2009**, *11* (10), 1865-1868.
5
6 (8) Diaz-Morales, O.; Calle-Vallejo, F.; de Munck, C.; Koper, M. T. M.,
7 Electrochemical Water Splitting by Gold: Evidence for an Oxide Decomposition
8 Mechanism. *Chem. Sci.* **2013**, *4* (6), 2334-2343.
9
10 (9) Doornkamp, C.; Ponec, V., The Universal Character of the Mars and Van
11 Krevelen Mechanism. *J. Mol. Catal. A: Chem.* **2000**, *162* (1-2), 19-32.
12
13 (10) Grimaud, A.; Demortiere, A.; Saubanere, M.; Dachraoui, W.; Duchamp, M.;
14 Doublet, M.-L.; Tarascon, J.-M., Activation of Surface Oxygen Sites on an
15 Iridium-Based Model Catalyst for the Oxygen Evolution Reaction. *Nat. Energy*
16 **2016**, *2* (1), 16189.
17
18 (11) Costentin, C.; Nocera, D. G., Self-healing Catalysis in Water. *Proc. Natl. Acad. Sci.*
19 *U.S.A.* **2017**, *114* (51), 13380-13384.
20
21 (12) Chang, S. H.; Danilovic, N.; Chang, K.-C.; Subbaraman, R.; Paulikas, A. P.; Fong, D.
22 D.; Highland, M. J.; Baldo, P. M.; Stamenkovic, V. R.; Freeland, J. W. *et al.*,
23 Functional Links Between Stability and Reactivity of Strontium Ruthenate Single
24 Crystals during Oxygen Evolution. *Nat. Commun.* **2014**, *5*, 4191
25
26 (13) Kasian, O.; Grote, J.-P.; Geiger, S.; Cherevko, S.; Mayrhofer, K. J. J., The Common
27 Intermediates of Oxygen Evolution and Dissolution Reactions during Water
28 Electrolysis on Iridium. *Angew. Chem., Int. Ed. Engl.* **2018**, *57* (9), 2488-2491.
29
30 (14) Giordano, L.; Han, B.; Risch, M.; Hong, W. T.; Rao, R. R.; Stoerzinger, K. A.;
31 Shao-Horn, Y., pH Dependence of OER Activity of Oxides: Current and Future
32 Perspectives. *Catalysis Today* **2016**, *262*, 2-10.
33
34 (15) Grimaud, A.; Hong, W. T.; Shao-Horn, Y.; Tarascon, J. M., Anionic Redox
35 Processes for Electrochemical Devices. *Nat. Mater.* **2016**, *15* (2), 121-126.
36
37 (16) Yang, C.; Laberty-Robert, C.; Batuk, D.; Cibin, G.; Chadwick, A. V.; Pimenta, V.;
38 Yin, W.; Zhang, L.; Tarascon, J. M.; Grimaud, A., Phosphate Ion Functionalization
39 of Perovskite Surfaces for Enhanced Oxygen Evolution Reaction. *J. Phys. Chem.*
40 *Lett.* **2017**, *8* (15), 3466-3472.
41
42 (17) Trzeźniewski, B. J.; Diaz-Morales, O.; Vermaas, D. A.; Longo, A.; Bras, W.; Koper,
43 M. T. M.; Smith, W. A., *In Situ* Observation of Active Oxygen Species in
44 Fe-Containing Ni-Based Oxygen Evolution Catalysts: The Effect of pH on
45 Electrochemical Activity. *J. Am. Chem. Soc.* **2015**, *137* (48), 15112-15121.
46
47 (18) Hong, W. T.; Stoerzinger, K. A.; Lee, Y.-L.; Giordano, L.; Grimaud, A.; Johnson, A.
48 M.; Hwang, J.; Crumlin, E. J.; Yang, W.; Shao-Horn, Y.,
49 Charge-transfer-energy-dependent Oxygen Evolution Reaction Mechanisms for
50 Perovskite Oxides. *Energy & Environmental Science* **2017**, *10* (10), 2190-2200.
51
52 (19) Yang, C.; Fontaine, O.; Tarascon, J. M.; Grimaud, A., Chemical Recognition of
53
54
55
56
57
58
59
60

- 1
2
3 Active Oxygen Species on the Surface of Oxygen Evolution Reaction
4 Electrocatalysts. *Angew. Chem. Int. Ed. Engl.* **2017**, *56* (30), 8652-8656.
- 5
6 (20) Spoeri, C.; Kwan, J. T. H.; Bonakdarpour, A.; Wilkinson, D.; Strasser, P., The
7 Stability Challenges of Oxygen Evolving Electrocatalysts: Towards a Common
8 Fundamental Understanding and Mitigation of Catalyst Degradation. *Angew.*
9 *Chem. Int. Ed. Engl.* **2017**, *56*, 5994.
- 10
11 (21) Rong, X.; Parolin, J.; Kolpak, A. M., A Fundamental Relationship between
12 Reaction Mechanism and Stability in Metal Oxide Catalysts for Oxygen
13 Evolution. *ACS Catalysis* **2016**, *6* (2), 1153-1158.
- 14
15 (22) Han, B.; Stoerzinger, Kelsey A.; Tileli, V.; Gamalski, Andrew D.; Stach, Eric A.;
16 Shao-Horn, Y., Nanoscale Structural Oscillations in Perovskite Oxides Induced by
17 Oxygen Evolution. *Nat. Mater.* **2016**, *16* (1), 121-126.
- 18
19 (23) Chang, S. H.; Connell, J. G.; Danilovic, N.; Subbaraman, R.; Chang, K.-C.;
20 Stamenkovic, V. R.; Markovic, N. M., Activity–Stability Relationship in the
21 Surface Electrochemistry of the Oxygen Evolution Reaction. *Faraday Discuss.*
22 **2014**, *176*, 125-133.
- 23
24 (24) Kanan, M. W.; Nocera, D. G., In situ Formation of an Oxygen-evolving Catalyst in
25 Neutral Water Containing Phosphate and Co^{2+} . *Science* **2008**, *321* (5892),
26 1072-1075.
- 27
28 (25) Kanan, M. W.; Surendranath, Y.; Nocera, D. G., Cobalt–phosphate
29 Oxygen-evolving Compound. *Chem. Soc. Rev.* **2009**, *38* (1), 109-114.
- 30
31 (26) Trotochaud, L.; Young, S. L.; Ranney, J. K.; Boettcher, S. W., Nickel–Iron
32 Oxyhydroxide Oxygen-Evolution Electrocatalysts: The Role of Intentional and
33 Incidental Iron Incorporation. *J. Am. Chem. Soc.* **2014**, *136* (18), 6744-6753.
- 34
35 (27) Man, I. C.; Su, H.-Y.; Calle-Vallejo, F.; Hansen, H. A.; Martínez, J. I.; Inoglu, N. G.;
36 Kitchin, J.; Jaramillo, T. F.; Nørskov, J. K.; Rossmeisl, J., Universality in Oxygen
37 Evolution Electrocatalysis on Oxide Surfaces. *ChemCatChem* **2011**, *3* (7),
38 1159-1165.
- 39
40 (28) May, K. J.; Carlton, C. E.; Stoerzinger, K. A.; Risch, M.; Suntivich, J.; Lee, Y.-L.;
41 Grimaud, A.; Shao-Horn, Y., Influence of Oxygen Evolution during Water
42 Oxidation on the Surface of Perovskite Oxide Catalysts. *J. Phys. Chem. Lett.*
43 **2012**, *3* (22), 3264-3270.
- 44
45 (29) Friebel, D.; Louie, M. W.; Bajdich, M.; Sanwald, K. E.; Cai, Y.; Wise, A. M.; Cheng,
46 M.-J.; Sokaras, D.; Weng, T.-C.; Alonso-Mori, R. *et al.*, Identification of Highly
47 Active Fe Sites in (Ni,Fe)OOH for Electrocatalytic Water Splitting. *J. Am. Chem.*
48 *Soc.* **2015**, *137* (3), 1305-1313.
- 49
50 (30) Köhler, L.; Ebrahimizadeh Abrishami, M.; Roddatis, V.; Geppert, J.; Risch, M.,
51 Mechanistic Parameters of Electrocatalytic Water Oxidation on LiMn_2O_4 in
52
53
54
55
56
57
58
59
60

- 1
2
3
4 Comparison to Natural Photosynthesis. *ChemSusChem* **2017**, *10* (22),
5 4479-4490.
- 6
7 (31) Filimonenkov, I. S.; Istomin, S. Y.; Antipov, E. V.; Tsirlina, G. A.; Savinova, E. R.,
8 Rotating Ring-Disk Electrode as a Quantitative Tool for the Investigation of the
9 Oxygen Evolution Reaction. *Electrochimica Acta* **2018**, *286*, 304-312.
- 10
11 (32) Abou-Warda, S.; Pietzuch, W.; Berghöfer, G.; Kesper, U.; Massa, W.; Reinen, D.,
12 Ordered K_2NiF_4 Structure of the Solids $La_2Li_{1/2}M_{1/2}O_4$ (M(III)=Co, Ni, Cu) and the
13 Bonding Properties of the MO_6 Polyhedra in Various Compounds of This Type.
14 *Journal of Solid State Chemistry* **1998**, *138* (1), 18-31.
- 15
16 (33) Goerlin, M.; Chernev, P.; Ferreira de Araujo, J.; Reier, T.; Dresch, S.; Paul, B.;
17 Kraehnert, R.; Dau, H.; Strasser, P., Oxygen Evolution Reaction Dynamics,
18 Faradaic Charge Efficiency, and the Active Metal Redox States of Ni-Fe Oxide
19 Water Splitting Electrocatalysts. *J. Am. Chem. Soc.* **2016**, *138* (17), 5603-5614.
- 20
21 (34) Goldsmith, Z. K.; Harshan, A. K.; Gerken, J. B.; Vörös, M.; Galli, G.; Stahl, S. S.;
22 Hammes-Schiffer, S., Characterization of NiFe Oxyhydroxide Electrocatalysts by
23 Integrated Electronic Structure Calculations and Spectroelectrochemistry. *Proc.*
24 *Natl. Acad. Sci. U.S.A.* **2017**, *114* (12), 3050-3055.
- 25
26 (35) Zhou, W.; Sunarso, J., Enhancing Bi-functional Electrocatalytic Activity of
27 Perovskite by Temperature Shock: A Case Study of $LaNiO_{3-\delta}$. *J. Phys. Chem. Lett.*
28 **2013**, *4* (17), 2982-2988.
- 29
30 (36) Wang, W.; Luo, J.; Chen, S., Carbon Oxidation Reactions Could Misguide the
31 Evaluation of Carbon Black-based Oxygen-evolution Electrocatalysts. *Chem.*
32 *Commun.* **2017**, *53* (84), 11556-11559.
- 33
34 (37) Risch, M.; Grimaud, A.; May, K. J.; Stoerzinger, K. A.; Chen, T. J.; Mansour, A. N.;
35 Shao-Horn, Y., Structural Changes of Cobalt-Based Perovskites upon Water
36 Oxidation Investigated by EXAFS. *J. Phys. Chem. C* **2013**, *117* (17), 8628-8635.
- 37
38 (38) Grimaud, A.; Diaz-Morales, O.; Han, B.; Hong, W. T.; Lee, Y. L.; Giordano, L.;
39 Stoerzinger, K. A.; Koper, M. T. M.; Shao-Horn, Y., Activating Lattice Oxygen
40 Redox Reactions in Metal Oxides to Catalyse Oxygen Evolution. *Nat. Chem.*
41 **2017**, *9* (5), 457-465.
- 42
43 (39) Schmies, H.; Bergmann, A.; Drnec, J.; Wang, G.; Teschner, D.; Köhl, S.; Sandbeck,
44 D. J. S.; Cherevko, S.; Gocyla, M.; Shviro, M. *et al.*, Unravelling Degradation
45 Pathways of Oxide-Supported Pt Fuel Cell Nanocatalysts under In Situ Operating
46 Conditions. *Adv. Energy Mater.* **2018**, *8* (4), 1701663.
- 47
48 (40) Yeo, B. S.; Klaus, S. L.; Ross, P. N.; Mathies, R. A.; Bell, A. T., Identification of
49 Hydroperoxy Species as Reaction Intermediates in the Electrochemical
50 Evolution of Oxygen on Gold. *ChemPhysChem* **2010**, *11*, 1854-1857.
- 51
52 (41) Kim, Y.-T.; Lopes, P. P.; Park, S.-A.; Lee, A. Y.; Lim, J.; Lee, H.; Back, S.; Jung, Y.;

1
2
3 Danilovic, N.; Stamenkovic, V.; Erlebacher, J.; Snyder, J.; Markovic, N. M.,
4 Balancing Activity, Stability and Conductivity of Nanoporous Core-shell
5 Iridium/Iridium Oxide Oxygen Evolution Catalysts. *Nat. Commun.* **2017**, 8 (1),
6 1449.
7
8
9
10
11
12
13
14
15
16
17
18
19
20
21
22
23
24
25
26
27
28
29
30
31
32
33
34
35
36
37
38
39
40
41
42
43
44
45
46
47
48
49
50
51
52
53
54
55
56
57
58
59
60